Electronic Supplementary Material (ESI) for Physical Chemistry Chemical Physics.

Adsorption of Amphiphilic Graft Copolymers in Solvents Selective for the Grafts on a Lyophobic Surface: A Coarse-Grained Simulation Study

Zbyšek Posel[1,3], Martin Svoboda[2,3], Zuzana Limpouchová[4], Martin Lísal[2,3] and Karel Procházka[4]

ELECTRONIC SUPPLEMENTARY INFORMATION

[1]Department of Informatics, Faculty of Science, J. E. Purkinje University, České mládeže 8, 400 96 Ústí n. Lab., Czech Republic

[2]Department of Physics, Faculty of Science, J. E. Purkinje University, České mládeže 8, 400 96 Ústí n. Lab., Czech Republic

[3]Department of Molecular and Mesoscale Modelling, Institute of Chemical Process Fundamentals of CAS, v. v. i., Rozvojová 135/1, 165 02 Prague 6-Suchdol, Czech Republic

[4]Department of Physical and Macromolecular Chemistry, Faculty of Science, Charles University in Prague, 128 43 Albertov 6, Prague2, Czech Republic

S1. Dissipative Particle Dynamics

In a Dissipative Particle Dynamics (DPD) simulation [1-3], the actual material (solvents, a graft copolymer and walls) is modeled as a collection of point particles that represent lumps of the material. DPD particles are defined by a mass m_i, position $\boldsymbol{r}_i$, and velocity $\boldsymbol{v}_i$, and interact with each other via a force $\boldsymbol{F}$ that is written as the sum of a conservative force $\boldsymbol{F}^C$, dissipative force $\boldsymbol{F}^D$, and random force $\boldsymbol{F}^R$:

$$\boldsymbol{F} = \boldsymbol{F}^C + \boldsymbol{F}^D + \boldsymbol{F}^R \tag{S1}$$

$\boldsymbol{F}^C$ is given as the negative derivative of a particle coarse-grained potential, u^{CG}, i.e.,

$$\boldsymbol{F}^C = -\nabla_{\boldsymbol{r}} u^{CG} \tag{S2}$$

The remaining two forces, $\boldsymbol{F}^D$ and $\boldsymbol{F}^R$, which arise from degrees of freedom neglected by coarse-graining, are given by

$$\boldsymbol{F}_{ij}^D = -\gamma_{ij}\, \omega^D\left(r_{ij}\right)\left(\frac{\boldsymbol{r}_{ij}}{r_{ij}} \cdot \boldsymbol{v}_{ij}\right)\frac{\boldsymbol{r}_{ij}}{r_{ij}} \tag{S3}$$

$$\boldsymbol{F}_{ij}^R = \sigma_{ij}\, \omega^R\left(r_{ij}\right)\frac{\zeta_{ij}}{\sqrt{\Delta t}}\frac{\boldsymbol{r}_{ij}}{r_{ij}} \tag{S4}$$

where $\boldsymbol{r}_{ij} = \boldsymbol{r}_i - \boldsymbol{r}_j$ is the separation vector between particle i and particle j, $r_{ij} = \left|\boldsymbol{r}_{ij}\right|$, $\omega^D\left(r\right)$ and $\omega^R\left(r\right)$ are weight functions that vanish for $r \geq r_c$, r_c is the cut-off radius, γ_{ij} is the friction coefficient, σ_{ij} is the noise amplitude, $\boldsymbol{v}_{ij} = \boldsymbol{v}_i - \boldsymbol{v}_j$, $\xi_{ij} = \xi_{ji}$ is a Gaussian random number with zero mean and unit variance that is chosen independently for each pair of interacting particles, and Δt is the time step.

Español and Warren [4] showed that the system samples the canonical ensemble and obeys the fluctuation-dissipation theorem if the following relationships hold:

$$\omega^D\left(r\right) = \left[\omega^R\left(r\right)\right]^2 \tag{S5}$$

$$\sigma_{ij}^2 = 2\gamma_{ij}\, kT \tag{S6}$$

$\omega^D\left(r\right)$ and $\omega^R\left(r\right)$ are typically chosen [1] as

$$\omega^D(r) = \left[\omega^R(r)\right]^2 = \left(1 - \frac{r}{r_c}\right)^2 \qquad (r_{ij} < r_c)$$
$$= 0 \qquad (r \geq r_c) \tag{S7}$$

The evolution of DPD particles in time t is governed by Newton's equations of motion:

$$\frac{d\boldsymbol{r}_i}{dt} = \boldsymbol{v}_i(t)$$
$$m_i \frac{d\boldsymbol{v}_i}{dt} = \boldsymbol{F}_i(t) = \sum_{i \neq j} \left(\boldsymbol{F}_{ij}^C + \boldsymbol{F}_{ij}^D + \boldsymbol{F}_{ij}^R\right) \tag{S8}$$

Following Groot and Warren and others [1-4], we considered all the DPD particles to be purely repulsive and the ij-pairs of particles to interact via a soft repulsive potential

$$u_{ij}^{sr} = \frac{a_{ij}}{2} r_c \left(1 - \frac{r_{ij}}{r_c}\right)^2 \qquad (r_{ij} < r_c)$$
$$= 0 \qquad (r_{ij} \geq r_c) \tag{S9}$$

where a_{ij} is the maximum repulsion between particles i and j, $r_{ij} = r_i - r_j$ is the separation distance, and r_c is the cut-off radius. The backbone and graft segments are connected by harmonic spring potentials:

$$u_{i,i+1}^{hs} = \frac{K}{2}\left(r_{i,i+1} - r_0\right)^2 \tag{S10}$$

acting between adjacent particles i and $i+1$ in addition to the soft repulsive interaction. In Eq. (S10), K is the spring constant ($K = 4kT$, k is the Boltzmann constant and T is the temperature), and r_0 is the equilibrium distance (r_0=0).

A graft copolymer contains solvophobic backbone beads A that have the interaction with solvent s described by $\Delta a_{sA} = a_{sA} - a_{ss} > 0$, and solvophilic graft beads B with solvent interaction $\Delta a_{sB} = a_{sB} - a_{ss} = -5$. The interaction of the surface with graft beads is repulsive and those with the backbone is attractive, i.e., only the backbone can adsorb on the surface. Solvent

selectivity is controlled by varying the repulsion between solvent and backbone beads. Complete set of repulsion parameters is given in main paper. Here we only summarize the description of solvent quality to avoid the confusion. The solvent with $\Delta a_{sA} = 0$ is called the good solvent for the backbone (or good common solvent for the copolymer). All solvents with $\Delta a_{sA} > 0$ are poor solvents for the backbone or selective solvents for the grafts. We call the solvents with $\Delta a_{sA} = 1$, 2 and 3 as the moderately poor solvents for the backbone (or mild selective solvents for the grafts), the solvents with $\Delta a_{sA} = 4$ and 5 as poor solvent for the backbone (selective solvents for the grafts) and those with $\Delta a_{sA} = 6$ and 7 as very poor solvent for the backbone (very selective or strongly selective solvents for grafts).

S2. Bounce-Back Surface Boundary Conditions

Modelling of solid surfaces is not straightforward in DPD, see for example Refs. 5 to 7. Soft nature of the repulsion potential between beads cannot prevent fluid beads from penetrating surface boundaries. Therefore, an extra effort is needed to impose no-slip surface boundary conditions. In a well-accepted and successfully tested approach, the surface beads are represented by "frozen" beads with the same density as the fluid, which are fixed and are not taken into account in the integration of equations of motion. The motion of fluid beads approaching the surface is modelled as their reflection (bounce back) from the surface when they are about to penetrate the surface. The principle of the implementation of no-slip surface boundary conditions into the DPD simulation machinery is depicted in Figure S1, which shows the trajectory of a fluid bead which is approaching the solid surface. The bounce-back reflection scheme successfully suppresses unphysical fluctuations of fluid density close to the surface and correctly imposes no-slip surface boundary conditions.

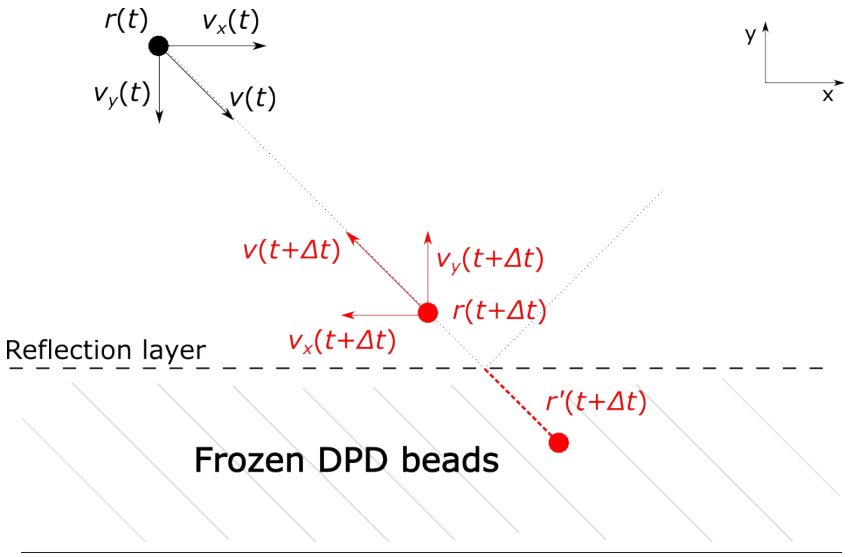

Figure S1: Schematic representation of bounce-back reflection between fluid and surface beads.

S3. Definition of Observables

The size of a graft copolymer was described by its radius of gyration, R_g, which is defined through the square radius of gyration [8]

$$R_g^2 = \frac{1}{N}\sum_{i=1}^{N}\left[(x_i - x_{com})^2 + (y_i - y_{com})^2 + (z_i - z_{com})^2\right] \tag{S11}$$

where N is the total number of beads of the graft copolymer, x_i, y_i and z_i are the Cartesian coordinates of bead i, and the subscript *com* denotes the centre of mass of the graft copolymer. A value of R_g was obtained as square root of the ensemble average of R_g^2. Besides R_g for the whole graft copolymer, we also computed the radius of gyration for the backbone, R_{gA}, via Eq. (S11) where N was replaced by the number of backbone beads N_A.

The graft copolymer in confined geometries can be further characterized by the radius of gyration parallel and perpendicular to the surface, $R_{g\parallel}$ and $R_{g\perp}$, respectively, which are given by expressions:

$$R_{g\parallel}^2 = \frac{1}{N}\sum_{i=1}^{N}(x_i - x_{com})^2 + (y_i - y_{com})^2 \tag{S12a}$$

$$R_{g\perp}^2 = \frac{1}{N}\sum_{i=1}^{N}(z_i - z_{com})^2 \tag{S12b}$$

Note that $R_g^2 = R_{g\parallel}^2 + R_{g\perp}^2$. The ratio of perpendicular and parallel components of R_g can then serve as an indicator if a graft copolymer is adsorbed or not, i.e.

$$\frac{R_{g\perp}^2}{R_{g||}^2}\begin{cases}\to 0: \textit{adsorption on the surface}\\ > 1: \textit{no adsorption on the surface}\end{cases} \tag{S13}$$

To further describe the adsorption of the graft copolymer onto the surface we measured the fraction of backbone segments within distance $2r_c$ from the surface, ϕ:

$$\phi = \frac{N_{A(adsorbed)}}{N_A} \tag{S14}$$

where $N_{A(adsorbed)}$ is total number of backbone beads within distance $2r_c$ from the surface [9].

The mobility of the graft copolymer was assessed by graft copolymer's centre-of-mass autocorrelation function

$$ACF_{com}(t) = \frac{\langle R_{com}(t_0)R_{com}(t_0+t)\rangle - \langle R_{com}(t_0)\rangle\langle R_{com}(t_0+t)\rangle}{\langle R_{com}(t_0)R_{com}(t_0)\rangle - \langle R_{com}(t_0)\rangle\langle R_{com}(t_0)\rangle} \quad \text{(S15)}$$

backbone's end-to-end distance autocorrelation function

$$ACF_e(t) = \frac{\langle R_e(t_0)R_e(t_0+t)\rangle - \langle R_e(t_0)\rangle\langle R_e(t_0+t)\rangle}{\langle R_e(t_0)R_e(t_0)\rangle - \langle R_e(t_0)\rangle\langle R_e(t_0)\rangle} \quad \text{(S16)}$$

and the corresponding autocorrelation times τ_{max}. In Eqs. (S15) and (S16), $R_{com} = |R_{com}|$, $R_e = |R_e|$, R_{com} and R_e are, respectively, the centre-of-mass position and end-to-end distance of the graft copolymer, and $\langle . \rangle$ denotes an ensemble average. Note that t_0 denotes the beginning of the time interval (t_0, $t_0 + t$), i.e., t_0 is a variable that runs over the whole simulation trajectory. For the weak and strong adsorption states, the autocorrelation functions were evaluated from the *x*- and *y*-components of $\boldsymbol{R}_{com}$ and $\boldsymbol{R}_e$, i.e., parallel with the wall. Values of τ_{max} were determined using the correlation time estimator $\tau(t)$.

$$\tau(t) = \frac{1}{2} + \sum_{k=1}^{N_{run}} ACF(k)\left(1 - \frac{k}{N_{run}}\right) \quad \text{(S17)}$$

where N_{run} are increasing numbers of simulation steps (corresponding to increasing time *t*) and $t = N_{\text{run}}\ N_{\text{step}}\ \Delta t$; N_{step}=1 000 is the number of time steps between two stored configurations and Δt=0.05. $\tau(t)$ typically increases with *t* and it reaches a plateau value which corresponds to a value of τ_{max} [10]. In addition for adsorption states, we computed the squared lateral displacement of copolymer's centre-of-mass

$$\Delta_{xy}^2(t) = [x_{com}(t) - x_{com}(t_0)]^2 + [y_{com}(t) - y_{com}(t_0)]^2 \quad \text{(S18)}$$

Determination of Δ_{xy}^2 includes averaging over different time origins t_0.

S4. Additional Results

To distinguish different systems studied, we denoted the particular systems as N_A-m-$N_B(\Delta a_{sA})$. So for example, 323-16-20(2) corresponds to a graft copolymer with N_A=323 backbone beads, spacing m=16, N_B=20 graft beads immersed in solvent with Δa_{sA}=2 for the solvent-backbone interactions. The same abbreviations are used for systems differing in the grafting density: LGC ("less grafted copolymers") for copolymers with the spacing m=8 and MGC ("more grafted copolymer") for copolymers with the spacing m=16.

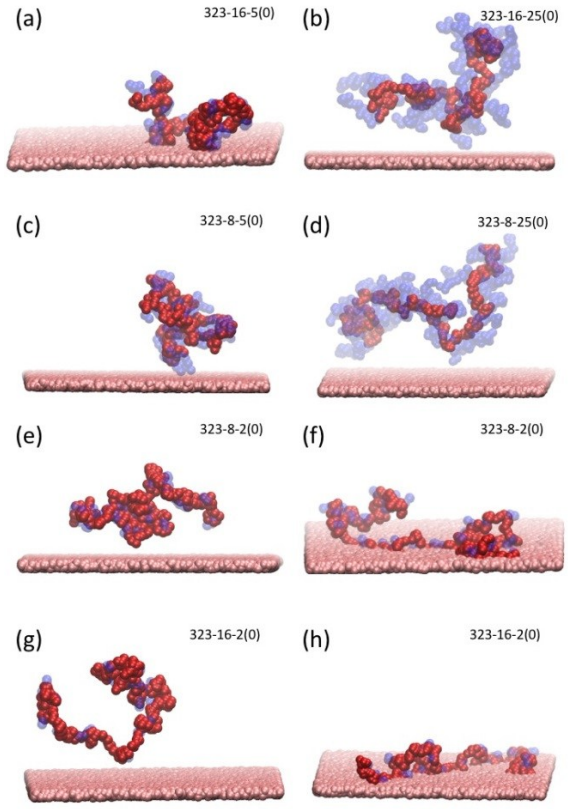

Figure S2: Simulation snapshots of graft copolymers under good solvent conditions Δa_{sA}=0. **(a)** Weak adsorption of LGC with short grafts, 323-16-5(0). **(b)** No adsorption of LGC with long grafts, 323-16-25(0). **(c)** No adsorption of graft copolymer densely grafted by short grafts, 323-8-5(0). **(d)** No adsorption of MGC with long grafts, 323-8-25(0). **(e)** and **(f)** show MGC with short grafts, 323-8-2(0), before and after adsorption on the surface, respectively. **(g)** and **(h)** display LGC with short grafts, 323-16-2(0), before and after adsorption, respectively. Red, blue and purple beads represent backbone, graft and wall segments, respectively. Solvent beads were omitted and graft beads were made transparent for the sake of clarity.

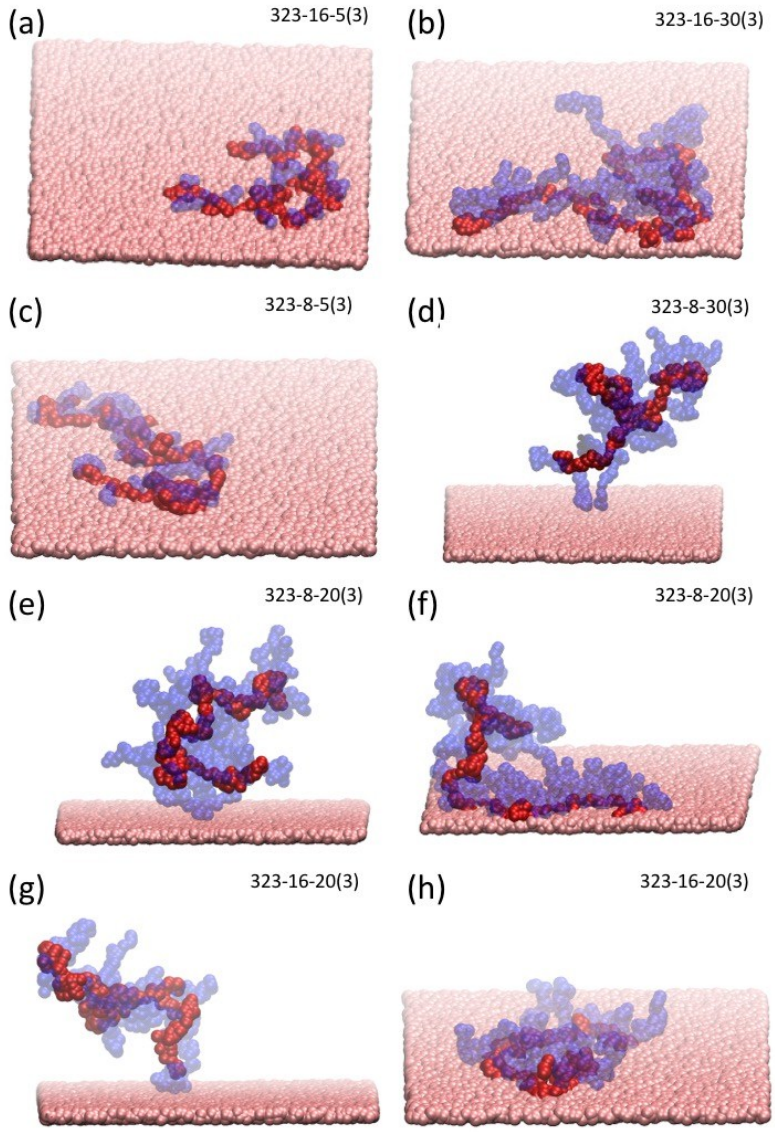

Figure S3: Simulation snapshots of graft copolymers under moderately poor solvent conditions Δa_{sA}=3. **(a)** Strong adsorption of LGC with short grafts, 323-16-5(3). **(b)** Strong adsorption of LGC with long grafts, 323-16-30(3). **(c)** Strong adsorption of MGC with short grafts, 323-8-5(3). **(d)** No adsorption of MGC with long grafts, 323-8-30(3). **(e)** and **(f)** show MGC with long grafts, 323-8-20(3), before and after adsorption on the surface, respectively. **(g)** and **(h)** display LGC with long grafts, 323-16-20(3), before and after adsorption, respectively. Red, blue and purple beads represent backbone, graft and wall segments, respectively. Solvent beads were omitted and graft beads were made transparent for the sake of clarity.

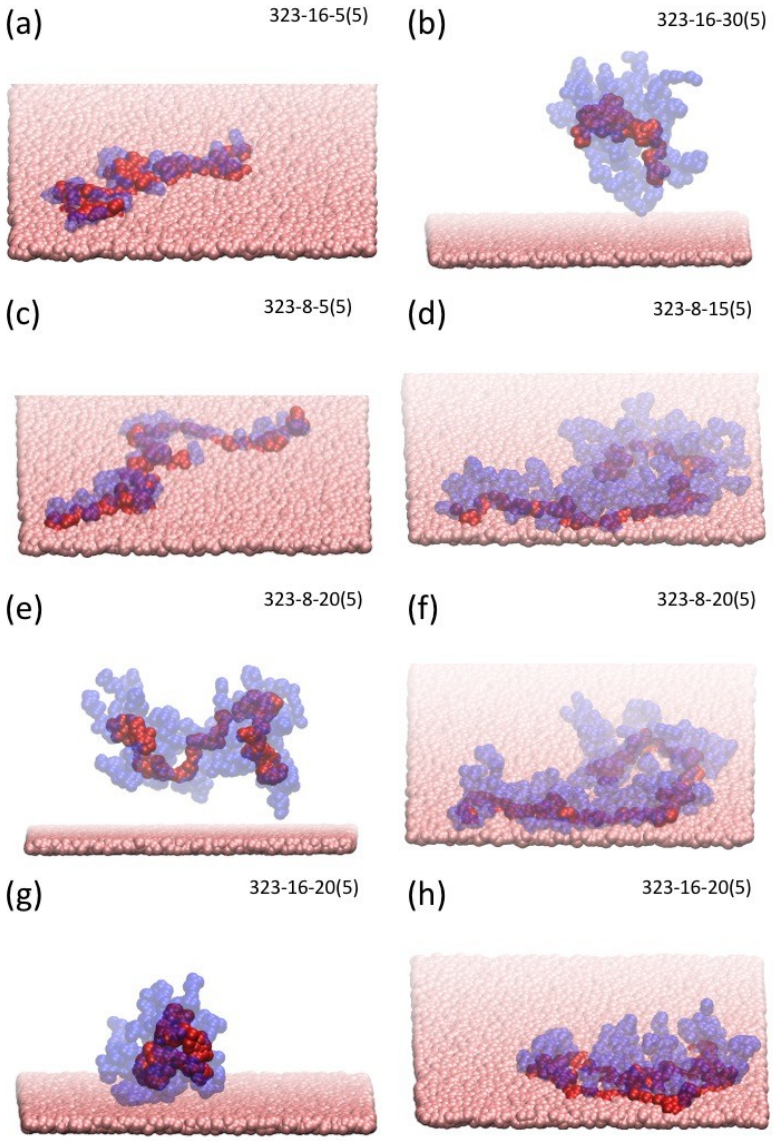

Figure S4: Simulation snapshots of graft copolymers under poor solvent conditions Δa_{sA}=5. **(a)** Strong adsorption of LGC with short grafts, 323-16-5(5). **(b)** No adsorption of LGC with long grafts, 323-16-30(5). **(c)** Strong adsorption of MGC with short grafts, 323-8-5(5). **(d)** Strong adsorption of MGC with moderately long grafts, 323-8-15(5). **(e)** and **(f)** show MGC with long grafts, 323-8-20(5), before and after adsorption on the surface, respectively. **(g)** and **(h)** display LGC with long grafts, 323-16-20(5), before and after adsorption, respectively. Red, blue and purple beads represent backbone, graft and wall segments, respectively. Solvent beads were omitted and graft beads were made transparent for the sake of clarity.

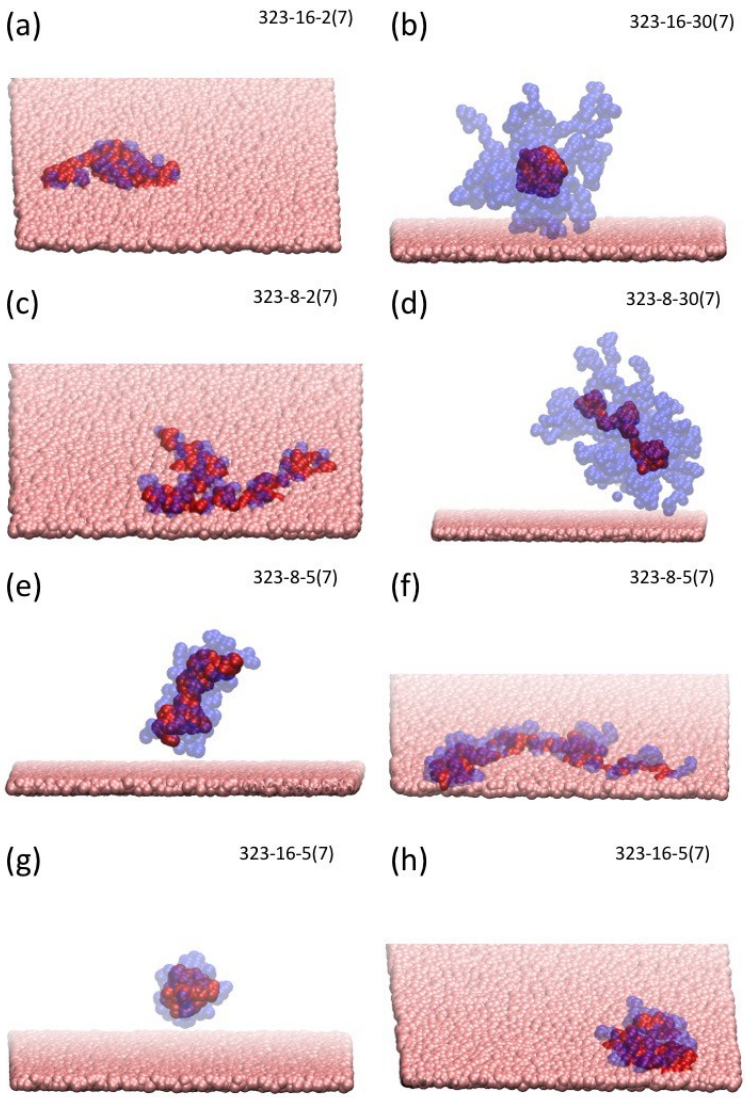

Figure S5: Simulation snapshots of graft copolymers under very poor solvent conditions Δa_{sA}=7. **(a)** Strong adsorption of LGC with short grafts, 323-16-2(7). **(b)** No adsorption of LGC with long grafts, 323-16-30(7). **(c)** Strong adsorption of MGC with short grafts, 323-8-2(7). **(d)** No adsorption of MGC with long grafts, 323-8-30(7). **(e)** and **(f)** show MGC with short grafts, 323-8-5(7), before and after adsorption on the surface, respectively. **(g)** and **(h)** display LGC with short grafts, 323-16-5(7), before and after adsorption, respectively. Red, blue and purple beads represent backbone, graft and wall segments, respectively. Solvent beads were omitted and graft beads were made transparent for the sake of clarity.

S5. Video Files

Video files illustrate typical scenarios observed in our simulations. They are labeled as *scenario*_N_A-m-N_B(Δa_{sA}) where *scenario* refers to state of graft copolymers such as micelle or adsorption.

Micelle_323-16-30(7): dynamics of LGC with long grafts under very poor solvent conditions forming a micelle. Red, blue and purple beads represent backbone, graft and wall segments, respectively. Solvent beads were omitted and graft beads were made transparent for the sake of clarity.

NecklaceMicelle_323-8-30(7): dynamics of MGC with long grafts under very poor solvent conditions forming a necklace of micelles. Red, blue and purple beads represent backbone, graft and wall segments, respectively. Solvent beads were omitted and graft beads were made transparent for the sake of clarity.

NoAdsorption_323-8-15(1): dynamics of MGC with moderately long grafts under moderately poor (slightly better than theta conditions, Δa_{sA}=1.64) solvent conditions not adsorbing onto the surface. Red, blue and purple beads represent backbone, graft and wall segments, respectively. Solvent beads were omitted and graft beads were made transparent for the sake of clarity.

WeakAdsorption_323-16-2(0): dynamics of LGC with short grafts under good solvent conditions weakly adsorbing onto the surface. Red, blue and purple beads represent backbone, graft and wall segments, respectively. Solvent beads were omitted and graft beads were made transparent for the sake of clarity.

WeakAdsorption_323-8-2(0): dynamics of MGC with short grafts under good solvent conditions weakly adsorbing onto the surface. Red, blue and purple beads represent backbone, graft and wall segments, respectively. Solvent beads were omitted and graft beads were made transparent for the sake of clarity.

StrongAdsorption_323-16-10(7): dynamics of LGC with short grafts under very poor solvent conditions strongly adsorbing onto the surface. Red, blue and purple beads represent backbone, graft and wall segments, respectively. Solvent beads were omitted and graft beads were made transparent for the sake of clarity.

StrongAdsorption_323-8-10(7): dynamics of MGC with short grafts under very poor solvent conditions strongly adsorbing onto the surface. Red, blue and purple beads represent backbone, graft and wall segments, respectively. Solvent beads were omitted and graft beads were made transparent for the sake of clarity.

StrongAdsorption_323-16-20(3): dynamics of LGC with long grafts under moderately poor solvent conditions strongly adsorbing onto the surface. Red, blue and purple beads represent backbone, graft and wall segments, respectively. Solvent beads were omitted and graft beads were made transparent for the sake of clarity.

StrongAdsorption_323-8-20(3): dynamics of MGC with long grafts under moderately poor solvent conditions strongly adsorbing onto the surface. Red, blue and purple beads represent backbone, graft and wall segments, respectively. Solvent beads were omitted and graft beads were made transparent for the sake of clarity.

S6. Mobility of the Graft Copolymer in Equilibrium States

We assessed mobility of the graft copolymer in the various regions of the phase diagram using the autocorrelation functions ACF_{com} and ACF_e, and correlation time τ_{max}. Figures S6, S7 and S8 display examples of ACFs for non-adsorption, weak and strong adsorption states, respectively. For the non-adsorption regions, we chose three systems: 323-16-20(0), 323-16-40(0), and 323-8-20(0). For the weak adsorption regions, we selected two systems: 323-16-20(1) and 323-8-20(2). For the strong adsorption regions, we picked two systems: 323-16-20(3) and 323-8-20(3).

Figure S9 then shows examples of $\tau(t)$ for the non-adsorption, weak and strong adsorption states where a plateau value in $\tau(t)$ at long time corresponds to a value of τ_{max}. We found that values of the correlation time ranged from $\tau_{max} \cong 200$ in the non-adsorption regions to $\tau_{max} \cong 2000$ in the strong adsorption region. Values of τ_{max} evaluated from ACF_{com} are two to three times shorter than the ones computed using ACF_e and they are by more than two orders smaller than the total length of simulations, $t_{run} = 150{,}000$ to 800,000. It is obvious that the mobility and flexibility of the strongly adsorbed system 323-16-20(3) are appreciably lower than those of the weakly adsorbed or non-adsorbed systems (corresponding values of τ_{max} are ca. four-times longer as compared with the weakly adsorbed and ca. eight-times longer as compared with the non-adsorbed chains). The conformation of the backbone (represented by its end-to-end distance) changes relatively slowly, but τ_{max} characterizing lateral motion of the adsorbed 323-16-20(3) chain on the surface is two-times shorter than that corresponding to fluctuation in backbone end-to-end distance. These τ_{max}values (more than two orders of magnitude smaller than the total length of the simulation run) prove that the adsorbed chains are not kinetically frozen and that the simulation yields reliable and well-equilibrated data.

Figure S10 shows examples of adsorption dynamics, $\phi(t)$, and squared lateral displacement, $\Delta_{xy}^2(t)$, for LGC and MGC systems in the strong adsorption regions. Note that time derivative of $\Delta_{xy}^2(t)$ is related to self-diffusivity of the graft copolymer. Fluctuations in ϕ and an increase of Δ_{xy}^2 with time indicate that the graft copolymer is not frozen on the surface but it diffuses along the surface. If a graft copolymer would be frozen on a surface its Δ_{xy}^2 would be constant.

(a)

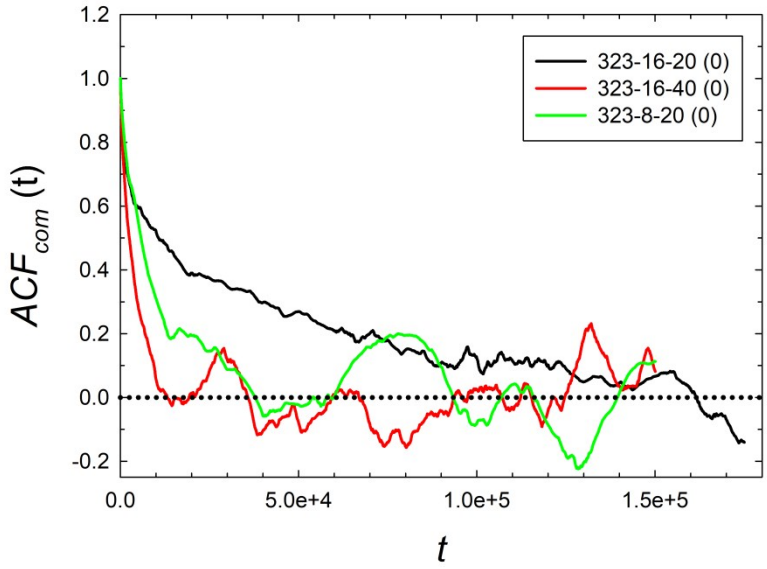

(b)

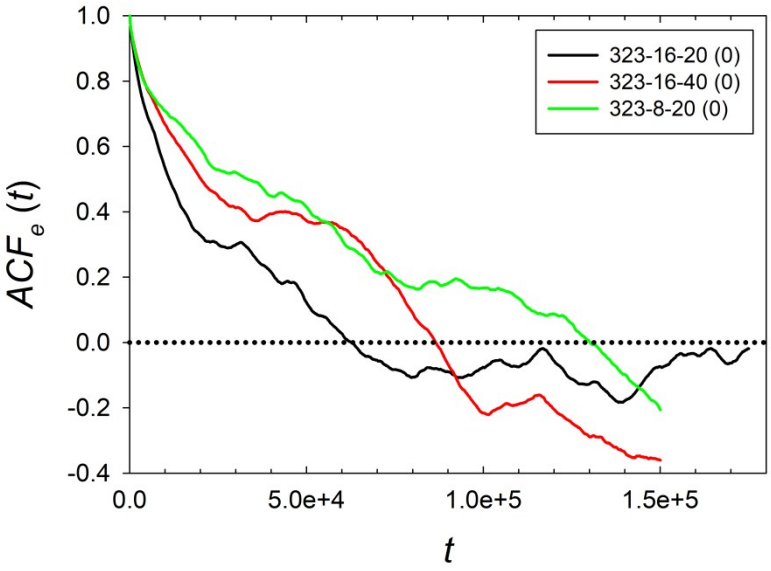

Figure S6: Examples of **(a)** graft copolymer's centre-of-mass autocorrelation function, ACF_{com}, and **(b)** backbone's end-to-end distance autocorrelation function, ACF_e, of the graft copolymer in the non-adsorption regions.

(a)

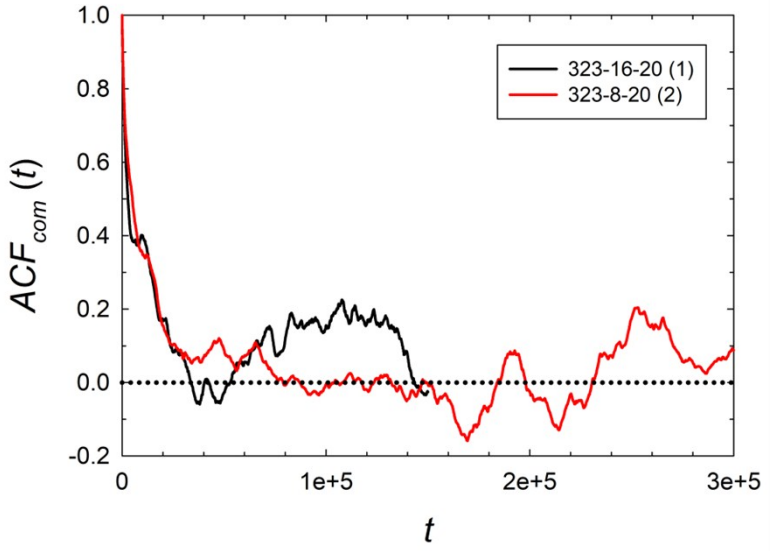

(b)

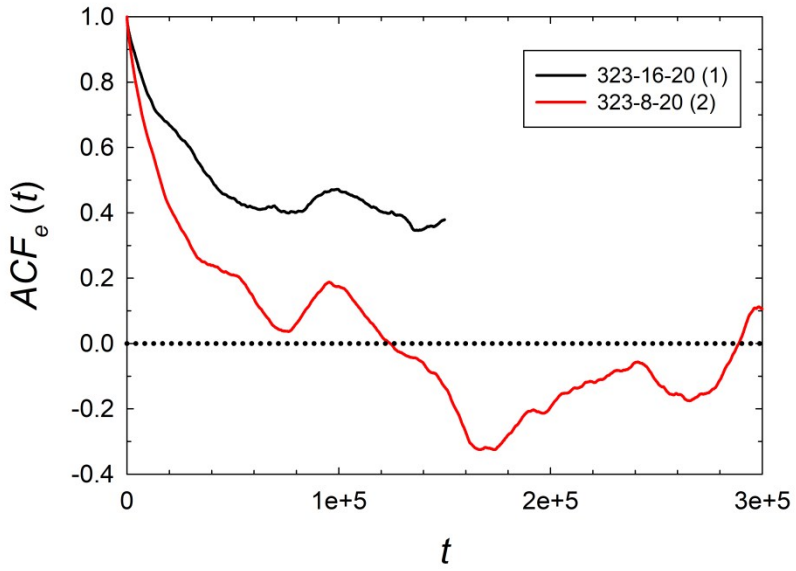

Figure S7: Examples of **(a)** graft copolymer's centre-of-mass autocorrelation function, ACF_{com}, and **(b)** backbone's end-to-end distance autocorrelation function, ACF_e, of the graft copolymer in the weak adsorption regions.

(a)

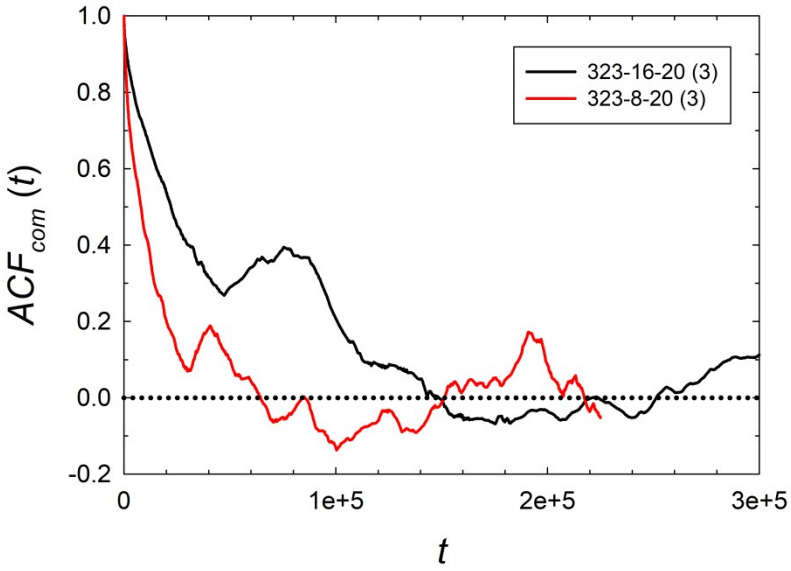

(b)

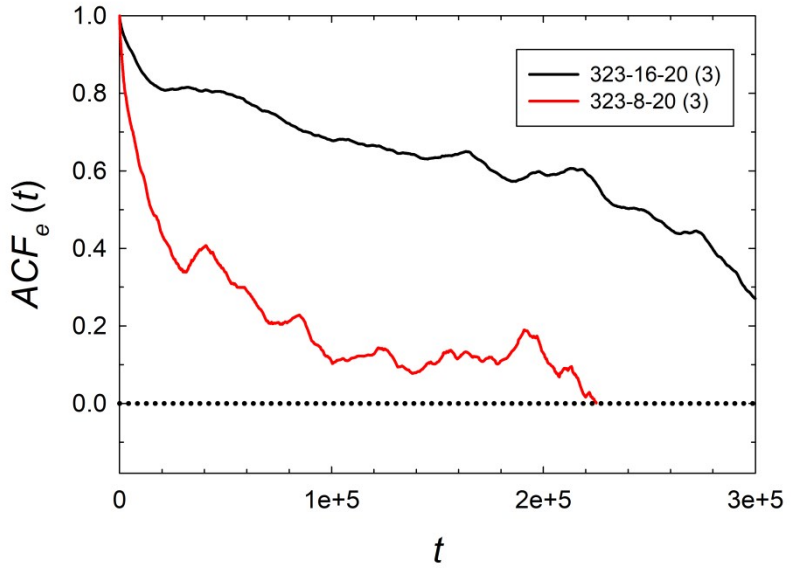

Figure S8: Examples of **(a)** graft copolymer's centre-of-mass autocorrelation function, ACF_{com}, and **(b)** backbone's end-to-end distance autocorrelation function, ACF_e, of the graft copolymer in the strong adsorption regions.

(a)

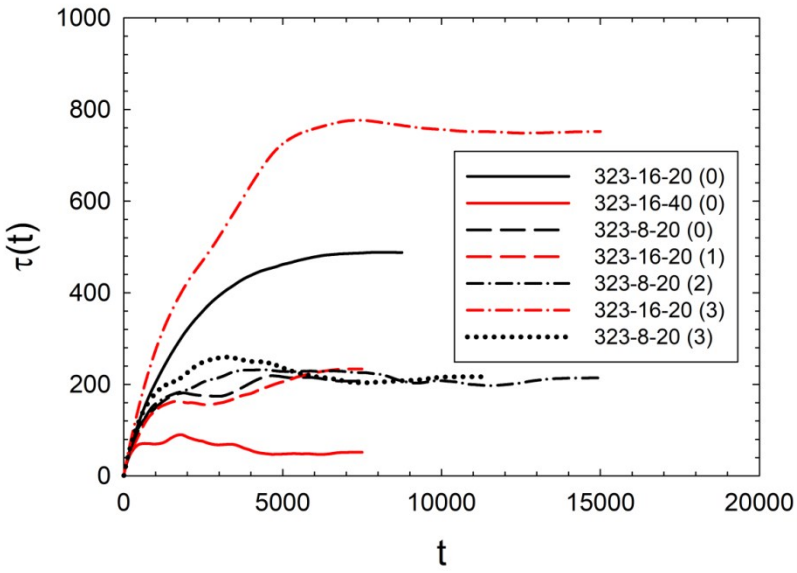

(b)

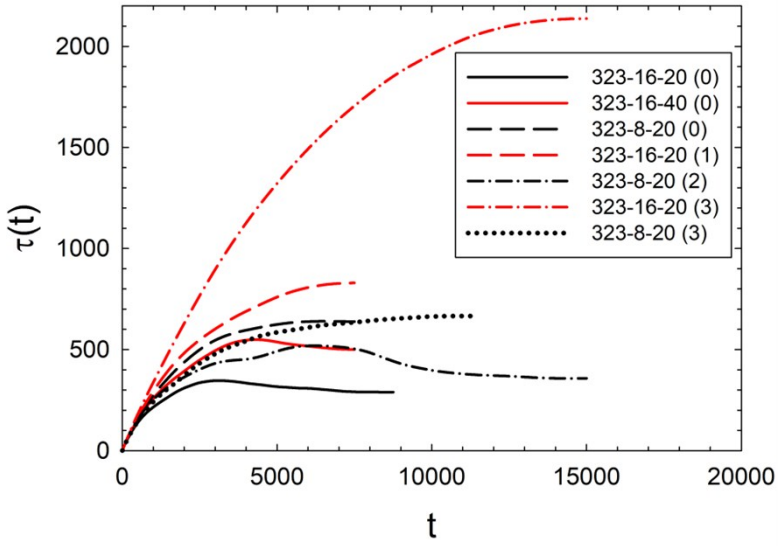

Figure S9: Examples of the correlation time estimator $\tau(t)$ evaluated from **(a)** the graft copolymer's centre-of-mass autocorrelation function, ACF_{com} and **(b)** the backbone's end-to-end distance autcorrelation function, ACF_e, for the graft copolymer in the non-adsorption, and weak and strong adsorption regions. A plateau value in $\tau(t)$ at long time corresponds to a value of the correlation time τ_{max}.

(a)

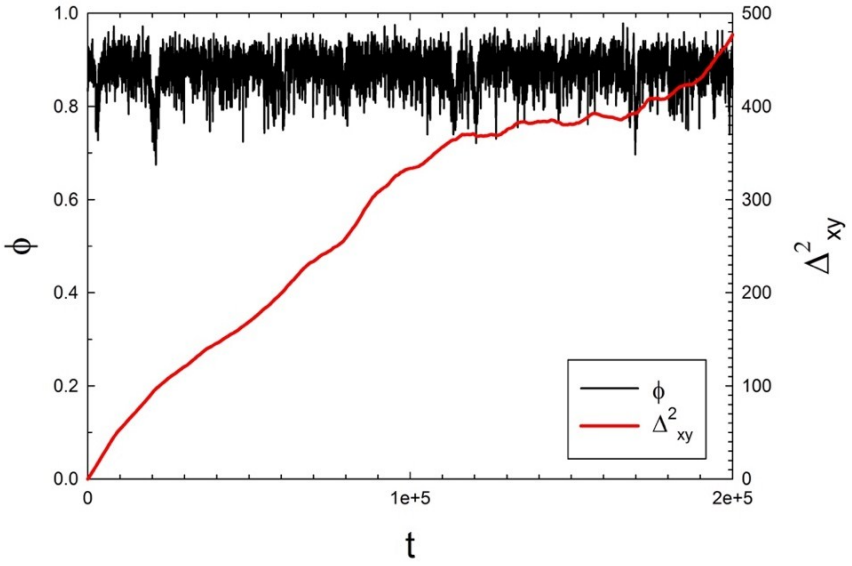

(b)

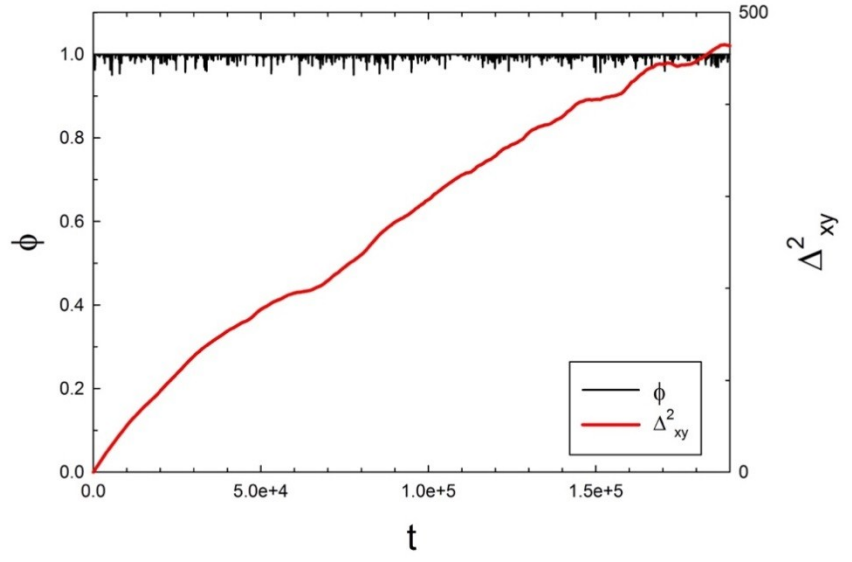

Figure S10: Examples of adsorption dynamics $\phi(t)$ and squared lateral displacement of copolymer's centre-of-mass, $\Delta^2_{xy}(\Delta t)$, for **(a)** MGC 323-8-20(3) and **(b)** LGC 323-16-20(3) adsorbed on the surface. Panels (a) and (b) display only a part of equilibrium trajectories.

S7. Dynamics of the Adsorption Process

In order to complete the discussion of the sorption dynamics and to give some pieces of information necessary for better understanding of the section ”Results and Discussion”, we present several simulation trajectories from the very beginning because they allow to compare the periods necessary for the first sorption-producing contact of the copolymer with the surface and the dynamics which follows. As mentioned in the paper, the conformations are generated with correct probabilities how they occur in the canonical ensemble, hence the period necessary for the “first capture” of the chain by the attractive surface indicate in a good approximation how readily the chains in the vicinity of the surface are adsorbed. It means that the length of the initial period before the adsorption (together with the inspection of the conformations that precede and follow the capture of the copolymer) provide valuable semi-quantitative information on the speed and mechanism of the sorption process. Even though this information is based on a single trajectory only, careful inspections of the whole trajectories allow one to judge how instantaneous conformations of chains approaching the attractive surface, which are influenced both by the bulk solvent quality and by polymer-surface interaction, affect the sorption process and how the copolymer-solvent interactions compete with copolymer-surface interactions.

Because the Figures S3 to S6 are discussed in detail in pertinent parts of “Results and Discussion”, here we present only the simulation data with appropriate legends and refer the reader to the main text.

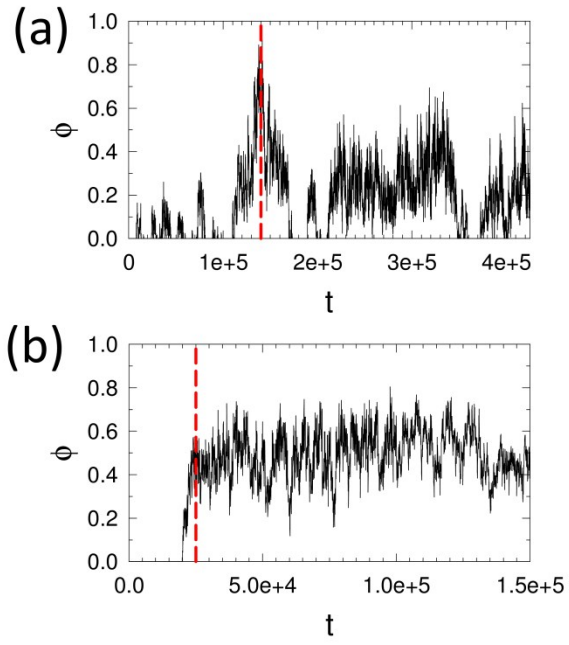

Figure S11: Adsorption dynamics of graft copolymers with the graft lengths N_B=2 in good solvent for the backbone, Δa_{sA}=0 for (**a**) MGC (m=8), and (**b**) LGC (m=16), respectively. The vertical lines denote the boundary where we started to evaluate the ensemble averages.

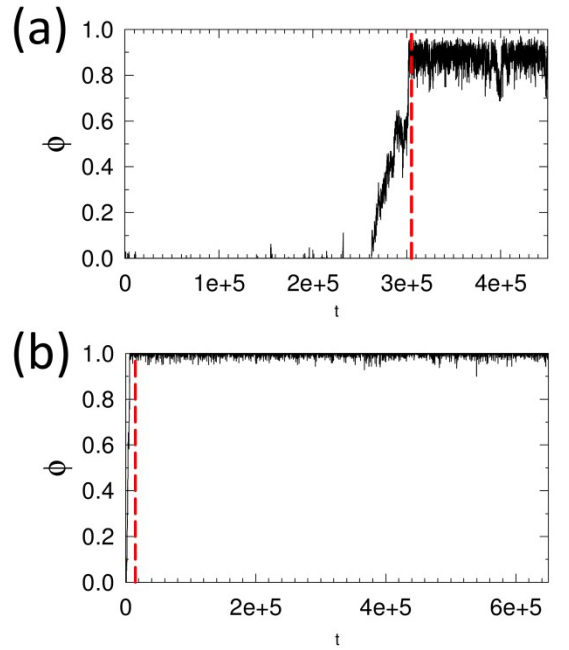

Figure S12: Adsorption dynamics of graft copolymers with the graft lengths N_B=20 in moderately poor solvent for the backbone, Δa_{sA}=3 for (**a**) MGC (m=8), and (**b**) LGC (m=16), respectively. The vertical lines denote the boundary where we started to evaluate the ensemble averages.

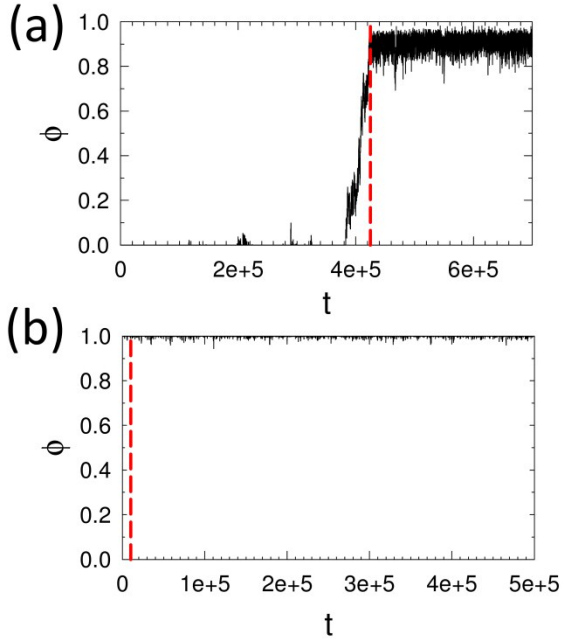

Figure S13: Adsorption dynamics of graft copolymers with the graft lengths N_B=20 in poor solvent for the backbone, Δa_{sA}=5 for (**a**) MGC (m=8), and (**b**) LGC (m=16), respectively. The vertical lines denote the boundary where we started to evaluate the ensemble averages.

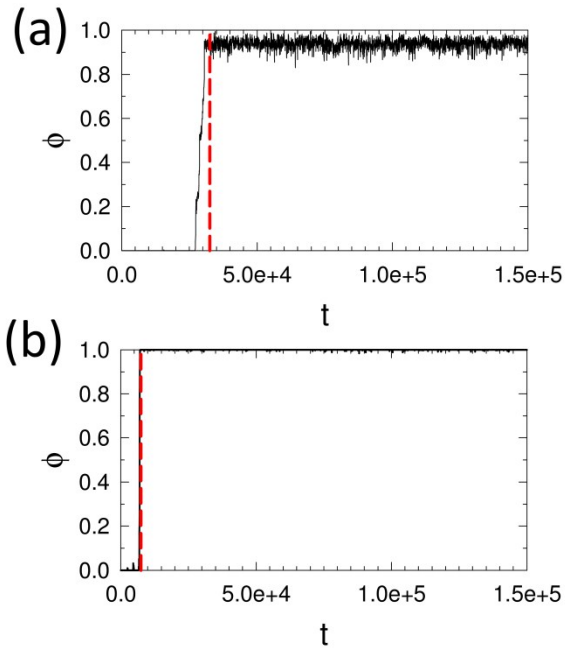

Figure S14: Adsorption dynamics of graft copolymers with the graft lengths N_B=5 in very poor solvent for the backbone, Δa_{sA}=7 for (**a**) MGC (m=8), and (**b**) LGC (m=16), respectively. The vertical lines denote the boundary where we started to evaluate the ensemble averages.

S8. References

[1] R. D. Groot, P. B. Warren, J. Chem. Phys. 107 (1997) 4423-4435.

[2] P. J. Hoogerbrugge, J. M. V. A. Koelman, Europhys. Lett. 19 (1992) 155-160.

[3] J. M. V. A. Koelman, P. J. Hoogerbrugge, Europhys. Lett. 21 (1993) 363-368.

[4] P. Espaňol, P. B. Warren, Europhys. Lett. 30 (1995) 191-196.

[5] I. V. Pivkin, G. E. Karniadakis, J. Comput. Phys. 207 (2005) 114-128.

[6] Z. Posel, M. Svoboda, C. M. Colina, M. Lísal, Soft Matter 13 (2017) 1634-1645.

[7] N. A. Gatsonis, R. Potami, J. Yang, J. Comput. Phys. 256 (2014) 441-464.

[8] M. Rubinstein, R. H. Colby, Polymer Physics, New York: Oxford University, 2003.

[9] L. I. Klushin, A. A. Polotsky, H. Hsu, D. A. Markelov, K. Binder, A. M. Skvortsov, Phys. Rev. E 87 (2013) 22604-22619.

[10] W. Janke, Statistical analysis of simulations: Data correlations and error estimation, in Quantum Simulations of Complex Many-Body Systems: From Theory to Algorithms, in J. Grotendorst, D. Marx and A. Muramatsu (eds.), Lecture Notes, John von Neumann Institute for Computing, Jülich, NIC Series, Vol. 10, pp. 423-445, 2002.